Explicit/implicit multi-time step co-simulation in unbounded medium with Rayleigh damping and application for wave barrier

Sijia Li, Michael Brun, Irini Djeran-Maigre, Sergey Kuznetsov

Explicit/implicit multi-time step co-simulation in unbounded medium with Rayleigh damping and application for wave barrier

Sijia Li[a], Michael Brun[a], Irini Djeran-Maigre[a] and Sergey Kuznetsov[b]

[a]GeoMaS, INSA Lyon, University of Lyon, Villeurbanne, France
[b]Institute for Problems in Mechanics, Moscow, Russia

Co-simulation strategies using both Abaqus/Explicit and Abaqus/Implicit are investigated for analysing wave propagation in two-dimensional unbounded soil domain. The co-simulation is based on the coupling GC method, allowing for coupling different finite element codes with differ-ent time integrators and time-scales depending on the partitions of the domain. Absorbing layers using increasing damping (ALID), based on Rayleigh viscous damping, are considered at the boundary to model the semi-infinite medium. The proposed absorbing region is called hybrid (different time integrators) asynchronous (different time steps) absorb-ing layers using increasing damping (HA-ALID). Lamb'stestand awave barrier problem are investigated. First, HA-ALID turns out to be more accurate than non-reflective conditions available in Abaqus/Explicit. Second, the critical time step in the domain of interest remains unaffected by the choice of damping characteristics in the HA-ALID, contrary to the case of a full explicit computation. Third, the time steps for the solid barrier and the HA-ALID are not restrained by the CFL con-dition imposed by the explicit partition for stability reasons. Because of its good accuracy and ability to be realized using only FE Abaqus pack-age, without a third-party software component, this strategy provides a wide range of applications in soil–structure interaction problems.

KEYWORDS
Hybrid asynchronous Rayleigh absorbing layers (HA-ALID); co-simulation; wave propagation; multi-physics; subdomain decomposition; interface; unbounded medium; wave barrier

Introduction

The isolation of buildings against shocks and propagating waves in the soil becomes a more and more important problem due to the increasing intensity of machine foundations or human activities such as railway and highway traffic. Moreover, modern equipments such as computers, accurate measurement instruments, may be affected by the induced vibrations. Finally, people who live near these disturbance sources become more sensitive to the industrial vibrations and cannot increase their tolerance for inconvenience and discomfort. Thus, there is a strong need to reduce vibration experienced by people, structures and equipments using isolation systems. Wave barriers corresponding to various obstacles such as open trenches and solid barriers composed of different materials (Çelebi et al., 2009) constitute examples of isolation measures which can be used against soil vibrations. The design of wave barriers motivated the development of analytical and numerical tools for analysing their isolating effect on travelling waves (Al-Hussaini

& Ahmad, 1991; Beskos, Dasgupta, & Vardoulakis, 1986). In most cases, the problem characterized by their complex geometry, boundary conditions, nonlinear material behavior laws for the soil is too difficult to be dealt with an analytical method, requiring the use of well-established numerical methods such as the finite element method (FEM) (Semblat, 1999).

One of the critical points of the numerical simulation of wave propagation problems in unbounded domains using the FEM is how to simulate infinite media. The simplest way is to consider a very large extended numerical mesh, but it leads to important computation times, in particular when long time duration excitations are considered. Hence non-reflective boundary conditions are required at the boundary of the truncated domain for mimicking infinite or semi-infinite media. Several kinds of artificial boundaries in numerical methods have been developed to avoid spurious waves reflected at the boundary, such as the infinite elements (Bettess, 1977; Nasri & Magnan, 1997; Su & Wang, 2013), absorbing boundary conditions (Enquist & Majda,1977), or perfect matched layers (PML). PML proposed by Bérenger (1994) is becoming increasingly used for dealing with infinite media in the context of finite difference and FEMs. The spatial (FEM) and time discrete formulation of PML proposed by Basu and Chopra (2010) has been recently reemployed by Brun, Zafati, Djeran-Maigre, and Prunier (2016) for extending the PML capabilities towards hybrid time integration (implicit time integration in the PML whereas the domain of interest is integrated using an explicit time integrator) and multi time steps (different times steps in the domain of interest and PML). Semblat, Lenti, and Gandomzadeh (2011) and Rajagopal, Drozdz, Skelton, Lowe, and Craster (2012) introduced more convenient techniques for implementing efficient absorbing conditions into commercial finite element codes, called absorbing layers using increasing damping (ALID), based on Rayleigh viscous damping matrix associated with an increasing damping ratio in the thickness of the absorbing region. Analytical models enabling to select the ALID parameters are developed by the authors to provide quick and valuable results, satisfying a desired accuracy. However, if an explicit time integration scheme is adopted both in the domain of interest and the Rayleigh absorbing layer, the introduction of Rayleigh matrix will decrease the value of the critical time step (Hughes, 1987). When there are complex structures in the domain of interest, it costs much more computation time. To avoid the critical time step in the domain of interest to be affected by introduction of Rayleigh matrix, the subdomain strategy proposed by Gravouil and Combescure (Combescure & Gravouil, 2002; Gravouil & Combescure, 2001) can be used to couple different schemes associated with different time steps depending on subdomains. Based on the GC coupling method, Zafati, Brun, Djeran-Maigre, and Prunier (2015) proposed a procedure for modelling infinite media using Rayleigh viscous damping. In short, the GC method is based on the gluing of velocities at the interface between two finite element partitions using a dual formulation by means of Lagrange multipliers. The velocity continuity condition is imposed at the fine time-scale, associated with the explicit time integration, whereas the implicit partition is associated with the large time scale. Globally speaking, the purpose of co-simulations is to be able to differently integrate in time partitions of a complex problem. Co-simulations have been successfully carried out in various applications: structure–structure interaction problem in structural dynamics (Brun, Batti, Limam, & Combescure, 2012; Brun, Batti, Limam, & Gravouil, 2012; Brun, Batti, Combescure, & Gravouil, 2014), soil–structure interaction (Brun, Gravouil, Combescure, & Limam, 2015) and fluid–structure interaction (Nunez-Ramirez, Marongiu, & Brun, 2017).

In this article, the strong form of wave propagation in a Rayleigh medium is first briefly presented, enabling us to derive improved relationships for mechanical parameters of the absorbing layers in order to minimize the wave reflection at the interface between the elastic medium and the Rayleigh medium. An efficient ALID can be set up, whose design depends on the desired target absorbing accuracy. Second, the weak formulation of the decomposed problem is obtained in order to derive the discretization in space and time algorithm able to couple Abaqus/Explicit with Abaqus/Implicit with their independent time steps. The proposed absorbing region is called hybrid (different time integrators) asynchronous (different time steps) ALID (HA-ALID), enabling

to integrate the absorbing layers using implicit time integrator and large time step. In numerical applications, Lamb's test is considered to assess the HA-ALID efficiency using Abaqus co-simulation: several profiles (linear, quadratic, square-root) of the damping ratio in the thickness of the HA-ALID are investigated so as to optimise the absorbing effect into the HA-ALID while minimising the spurious wave reflection at the interface with the elastic domain. The efficiency of the proposed method is compared with non-reflective conditions available in Abaqus/Explicit, highlighting the very good behaviour of the co-simulation strategy. Finally, a simulation of a wave barrier problem is carried out using the co-simulation and compared to an Abaqus/Explicit simulation with infinite elements with the same mesh for the domain of interest. Three partitions of the global problem have been handled in the most efficient way: the solid barrier made of concrete, the soil and the absorbing region, using the commercial Abaqus packages including both Abaqus/Standard and Abaqus/Explicit. Abaqus/Explicit is considered for reproducing the wave propagation into the soil, whereas Abaqus/Implicit is considered for the solid wave barrier as well as the absorbing region at the boundary of the truncated mesh. It is shown that the co-simulation allows adopting large time steps for the solid barrier and HA-ALID, whereas explicit time integration imposes fine time steps on the whole mesh due to the Courant–Friedrichs–Lewy (CFL) condition required for the stability of the explicit time integration scheme. Moreover, in comparison to the Abaqus/Explicit simulation, the hybrid (explicit/implicit) asynchronous (different time steps) strategy provides much more accurate results of engineering interest such as the reduction ratio of displacement due to the presence of the barrier.

Hybrid asynchronous Rayleigh absorbing layer

Wave propagation equations in a Rayleigh medium

Rayleigh absorbing layer aims at damping out all the incident waves from the domain of interest while minimising the spurious waves reflected at the boundary of the truncated domain. For this purpose, the optimal conditions at the interface between a non-dissipative elastic medium Ω_1 and a dissipative Rayleigh medium Ω_2 can be established by considering the continuous problem of wave propagation. A strong form for the wave propagation in the continuous dissipative medium Ω_2, corresponding to the introduction of the classical viscous Rayleigh damping matrix into the classical semi-discretised of the equation of motion in three-dimensional medium, has been obtained by Zafati, Brun, Djeran-Maigre, and Prunier (2014). The displacement vector field $\underline{u_2}$ in the Rayleigh domain Ω_2 is given by the following equations:

$$\rho_2 \partial_t^2 \underline{u_2} + \alpha_M \rho_2 \partial_t \underline{u_2} = \mathrm{div}\left(\underline{\underline{\sigma_2}}(\underline{u_2})\right) \tag{1}$$

$$\underline{\underline{\sigma_2}} = \lambda_2 \mathrm{tr}\left(\underline{\underline{\varepsilon_2}}(\underline{u_2})\right) + 2\mu_2 \underline{\underline{\varepsilon_2}}(\underline{u_2}) + \alpha_K \left(\lambda_2 \mathrm{tr}\left(\underline{\underline{\varepsilon_2}}\left(\partial_t \underline{u_2}\right)\right) + 2\mu_2 \underline{\underline{\varepsilon_2}}\left(\partial t \underline{u_2}\right)\right) \tag{2}$$

$$\underline{\underline{\varepsilon_2}} = \frac{1}{2}\left[\mathrm{grad}(\underline{u_2}) + \mathrm{grad}(\underline{u_2})^T\right] \tag{3}$$

Equations (1)–(3) constitute the strong form of the wave propagation into a Rayleigh medium, σ_2, ε_2, λ_2, μ_2, ρ_2 being the stress matrix, strain matrix, Lamé coefficients, the density, Young's modulus and Poisson's ratio related to the Rayleigh domain Ω_2, respectively. It was shown that the parameters α_M and α_K introduced in Equations (1) and (2) correspond to the two classical parameters of the viscous Rayleigh damping matrix. Indeed, the classical expression of the Rayleigh matrix can be derived from the weak form of the previous equations as it will be shown in section 'Weak form and space discretization for HA-ALID'.

Next, the strong form of the wave propagation in Rayleigh medium is employed to obtain optimal conditions at the interface between an elastic domain Ω_1 and a dissipative Rayleigh medium Ω_2 so as to minimise the spurious wave reflections.

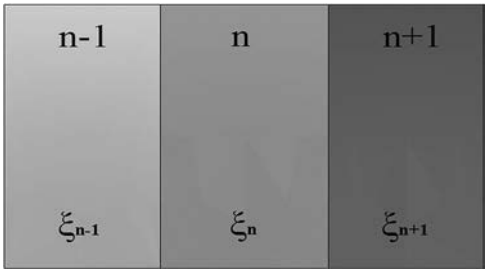

Figure 1. Layers in the absorbing subdomain.

ALID design

The argument is developed for one-dimensional wave propagation problem by distinguishing the P-waves and the S-waves in their strong form, written as

$$\rho_2\partial_t^2 u_2 + \alpha_M\rho_2\partial_t u_2 = (\lambda_2 + 2\mu_2)\partial_x^2 u_2 + \alpha_K(\lambda_2 + 2\mu_2)\partial_x^2\partial_t u_2 \mathrm{P-wave} \tag{4}$$

$$\rho_2\partial_t^2 u_2 + \alpha_M\rho_2\partial_t u_2 = \mu_2\partial_x^2 u_2 + \alpha_K\mu_2\partial_x^2\partial_t u_2 \mathrm{S-wave} \tag{5}$$

It was assumed that Rayleigh parameters can be obtained from a chosen damping ratio ξ and the dominant angular frequency ω_0 as: $\frac{\alpha_M}{\omega_0} = \alpha_K\omega_0 = \xi$.

After analytically solving the interface problem using the previous strong form, the relationship for minimising the spurious reflections at the interface can be obtained

$$\begin{cases} E_2 = \dfrac{E_1}{1+\xi^2} \\ \nu_2 = \nu_1 \\ \rho_2 = \rho_1 \end{cases} \tag{6}$$

where E_1 and E_2 are Young's moduli, ν_1 and ν_2 are Poisson's ratios, ρ_1 and ρ_2 are the densities of subdomains Ω_1 and Ω_2, respectively. The decay of the amplitude δ is expressed in a logarithmic form with respect to the thickness of the Rayleigh absorbing layer e as follows:

$$\delta = \ln\left(\frac{|u_2(x)|}{|u_2(x+\Delta x)|}\right) \tag{7}$$

The relationship between the logarithmic decrement, the thickness and the damping ratio of the Rayleigh absorbing layer is shown below

$$\delta = \frac{\omega_0\xi\Delta x}{V_1 p} \tag{8}$$

where Δx denotes the thickness of the medium, ξ the damping ratio of the Rayleigh absorbing layer and V_{1p} represents the velocity of P wave in the domain of interest (elastic domain Ω_1). For achieving a target value of the logarithmic decrement, we can use the relationship in Equation (8) to design the Rayleigh medium by choosing its damping ratio and thickness. The velocity of P waves is higher than the velocity of S waves in the same medium. In other words, based on the above relationships, in order to reach the same logarithmic decrement, the necessary layer thickness for damping out S waves is smaller than the one related to P waves. For the design of absorbing layer, the velocity of P waves will be chosen to make sure that all the waves can be attenuated according to the target decrement.

The ALID proposed by Semblat et al. (2011) and Rajagopal et al. (2012) are considered by tuning the elastic parameters of each layer depending on the selected damping ratio as given by the optimal conditions in Equation (6). The main idea is to divide the Rayleigh absorbing medium into several uniform layers as shown in Figure 1, so that the decrements produced by each layer can be multiplied. Because of the logarithmic form of decrement, the total logarithmic

decrement can be easily obtained. Due to the difference of damping ratio between subdomains Ω_1 and Ω_2, spurious waves will be produced, though optimal conditions given by Equation (6) are applied. Indeed, it is important to note that non-reflective conditions between an elastic and a Rayleigh medium were obtained under the following assumptions: 1D wave propagation (normal incidence), continuous setting in space and in time, harmonic waves. Thus, in a more general problem, after spatial and time discretization, Equation (6) provides only approximate conditions used for the ALID design.

It is crucial to control the difference of damping ratios between subdomains. Indeed the evolution of damping ratio in layers has an important influence on the efficiency of the ALID. Here, a nonlinear increase of damping ratio is adopted to achieve a better accuracy than a simple linear increase. The parameters of each layer satisfying the optimal conditions at each interface are given by

$$\begin{cases} E_2^{(i+1)} = \dfrac{1+\xi_i^2}{1+\xi_{i+1}^2} E_2^{(i)} \\ E_2^{(1)} = \dfrac{1}{1+\xi_1^2} E_1 \\ \nu_2^{(i)} = \nu_1 \\ \rho_2^{(i)} = \rho_1 \\ \xi_i = \xi_0 \left(\frac{x}{L}\right)^m \end{cases} \tag{9}$$

where $E_2^{(i)}$ denotes Young's modulus, ξ_i the damping ratio, $\nu_2^{(i)}$ Poisson's ratio, $\rho_2^{(i)}$ the density of each layer i in the subdomain Ω_2, m the power of the damping function, x the distance in the thickness of the ALID, L the thickness of the ALID including all sublayers (i). The total logarithmic decrement δ is written as follows:

$$\begin{cases} \delta_i = \dfrac{\xi_0 \omega_0}{V_1 p} \left(\dfrac{x}{L}\right)^m \Delta x \\ \delta = \int_0^L \dfrac{\xi_0 \omega_0}{V_1 p} \left(\dfrac{x}{L}\right)^m dx = \dfrac{\xi_0 \omega_0 L}{(m+1) V_1 p} \end{cases} \tag{10}$$

where δ_i represents the logarithmic decrement of each sublayer i, Δx represents the thickness of each layer which is assumed to be constant.

The reflection coefficient R is given by:

$$R = e^{-2\delta} \tag{11}$$

For example, if the goal is to reach a target logarithmic decrement $\delta = \ln$ (10), this means that 90% of the amplitude of the incident will be absorbed from the interface to the end of the damping layers. Next, the attenuation also occurs for the reflection process from the end of the damping layer towards the interface. Thus, the incident wave is attenuated by 99% in the ALID and the reflection coefficient R is theoretically equal to 1%, under the 1D harmonic wave propagation assumption and before the discretisation in time and in space. By calculating Equation (10) in the integral form, a new general design formula for the system of Rayleigh absorbing layers with reflection coefficient R is derived:

$$\xi_0 = \frac{(m+1)}{2L\omega_0} \times V_1 p \times \ln\left(\frac{1}{R}\right) \tag{12}$$

Weak form and space discretization for HA-ALID

The elastic wave propagation from an elastic non-dissipative medium to a Rayleigh medium should be discretized in space and in time. Let Ω be a bounded domain belonging to $\mathbb{R}^2$ with a

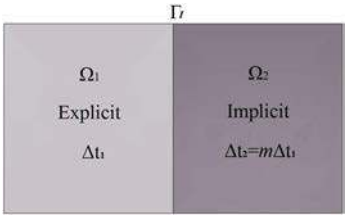

Figure 2. Domain Ω divided into two subdomains Ω_1 and Ω_2 with their material characteristics. Subdomain Ω_1 is handled by an explicit scheme with fine time step and subdomain Ω_2 by an implicit scheme with large time step.

regular boundary. $J = [0, T]$ is the time interval of interest. The domain Ω is divided into two partitions Ω_1 and Ω_2, as shown in Figure 2, such as: $\Omega_1 \cap \Omega_2 = \varnothing$ and $\partial\Omega_1 \cap \partial\Omega_2 = \Gamma_I$. Γ_I denotes the interface between the two subdomains, subdomain Ω_1 representing the non-dissipative medium (the domain of interest) and subdomain Ω_2 the Rayleigh medium.

The subdomain Ω_1 is characterised by its density ρ_1, Young's modulus E_1, Poisson coefficient ν_1, $\underline{b}_1$ the body force, $\underline{u}_1^D$ the Dirichlet prescribed displacement on Γ_1^D and $\underline{g}_1^N$ the traction force at the Neumann condition on Γ_1^N. The subdomain Ω_2 is characterized by its density ρ_2, Young's modulus E_2, Poisson coefficient ν_2, $\underline{b}_2$ the body force, $\underline{u}_2^D$ the Dirichlet prescribed displacement on Γ_2^D, $\underline{g}_2^N$ the traction force at the Neumann condition on Γ_2^N and the parameters α_M and α_K introduced in the strong form of the wave equation in Equations (1) and (2).

In order to write the weak form of the coupled problem in Ω divided into two partitions Ω_1 and Ω_2, test functions $\underline{\nu}_1$ and $\underline{\nu}_2$ belonging to the appropriate spaces W_1^* and W_2^* must be introduced:

$$\begin{cases} \underline{\nu}_1 \in W_1^*, W_1^* = \left\{ \underline{u}_1 \in \left(H^1(\Omega_1)\right)^d \text{ and } \underline{\nu}_1 = 0 \text{ on } \Gamma_1^D \right\} \\ \underline{\nu}_2 \in W_2^*, W_2^* = \left\{ \underline{u}_2 \in \left(H^1(\Omega_2)\right)^d \text{ and } \underline{\nu}_2 = 0 \text{ on } \Gamma_2^D \right\} \end{cases} \tag{13}$$

The solutions $\underline{u}_1$ and $\underline{u}_2$ belong to the appropriate spaces W_1 and W_2:

$$\begin{cases} \underline{u}_1(t) \in W_1, W_1 = \left\{ \underline{u}_1 \in \left(H^1(\Omega_1)\right)^d \text{ and } \underline{u}_1 = u_1^D \text{ on } \Gamma_1^D \right\} \\ \underline{u}_2 \in W_2, W_2 = \left\{ \underline{u}_2 \in \left(H^1(\Omega_2)\right)^d \text{ and } \underline{u}_2 = u_2^D \text{ on } \Gamma_2^D \right\} \end{cases} \tag{14}$$

where d is the space dimension (equal to 1, 2 or 3). The introduction of the Lagrange multiplier field allows us to glue the velocities of the two subdomains at the interface Γ_1. They belong to the adapted dual trace space Q, defined at the interface.

All the above considered space variables are assumed to be sufficiently smooth and regular. Using a dual Schur formulation, the principle of virtual power for transient dynamics can be written. Find the solution $\underline{u}1(t) \in W_1$, $\underline{u}_2(t) \in W_2$ and $\underline{\lambda}(t) \in Q$, for which the following weak form is satisfied $\forall \underline{\nu}_1 \in W_1^*, \forall \underline{\nu}_2 W_2^*$ and $\forall \underline{\mu} \in Q*$:

$$\begin{aligned} &\int_{\Omega_1} \rho_1 \underline{\nu}_1 \cdot \underline{\ddot{u}}_1 d\Omega + \int_{\Omega_1} \underline{\underline{\varepsilon}}(\underline{\nu}_1) : \underline{\underline{\sigma}}_1 d\Omega + \int_{\Omega_2} \rho_2 \underline{\nu}_2 \cdot \underline{\ddot{u}}_2 d\Omega + \int_{\Omega_2} \underline{\underline{\varepsilon}}(\underline{\nu}_2) : \underline{\underline{\sigma}}_2 d\Omega \\ &+\alpha_M \int_{\Omega_2} \rho_2 \underline{\nu}_2 \cdot \underline{\dot{u}}_2 d\Omega + \int_{\Gamma_1} \underline{\nu}_1 \cdot \underline{\lambda} d\Gamma + \int_{\Gamma_1} \underline{\nu}_2 \cdot \underline{\lambda} d\Gamma + \int_{\Gamma_1} \underline{\mu}_1 \cdot (\underline{\dot{u}}_1 - \underline{\dot{u}}_2) d\Gamma \\ &= \int_{\Omega_1} \underline{\nu}_1 \cdot \underline{b}_1 d\Omega + \int_{\Gamma_1^N} \underline{\nu}_1 \cdot \underline{g}_1^N d\Gamma + \int_{\Omega 2} \underline{\nu}_2 \cdot \underline{b}_2 d\Omega + \int_{\Gamma_2^N} \underline{\nu}_2 \cdot \underline{g}_2^N d\Gamma \end{aligned} \tag{15}$$

where the stress tensor $\underline{\underline{\varepsilon}}_2$ satisfies the behaviour law given in Equation (2). Then, we follow the classical lines of the finite element discretization. At the interface between the subdomains, the continuity of velocities is imposed by the following condition:

$$L_1\dot{U}_1 + L_2\dot{U}_2 = 0 \tag{16}$$

where L_1 and L_2 are the Boolean matrices in the case of matching meshes at the interface; they operate on nodal vectors associated with the two subdomains Ω_1 and Ω_2; they pick out the degrees of freedom belonging to the interface Γ_1 in order to ensure the kinematic continuity at the interface.

Thus the restricted velocities at the interface can be obtained from the global nodal velocity vectors $\dot{U}_1$ and $\dot{U}_2$ by the relationships:

$$\begin{cases} \dot{U}_1^{\Gamma} = L_1\dot{U}_1 \\ \dot{U}_2^{\Gamma} = L_2\dot{U}_2 \end{cases} \tag{17}$$

Same relationships hold for the global virtual nodal velocities V_1 and V_2. Thus interface terms involving the Lagrange multiplier field in Equation (15) can be expressed as:

$$\begin{cases} \int_{\Gamma_1} \underline{\nu}_1 \cdot \underline{\lambda} d\Gamma = V_1^T L_1^T \lambda \\ \int_{\Gamma_1} \underline{\nu}_2 \cdot \underline{\lambda} d\Gamma = V_2^T L_2^T \lambda \end{cases} \tag{18}$$

Time discretization of HA-ALID

For the time discretization, the GC method proposed by Gravouil and Combescure is employed (Combescure & Gravouil, 2002; Gravouil & Combescure, 2001). Adopting the continuity of velocities at the interface, it was demonstrated that the coupling GC method is stable for any Newmark integrators (implicit and explicit) with their own time step depending on subdomains. When adopting the same time step, second order of accuracy is achieved. It leads to the first order of accuracy when different time steps are adopted due to a slight spurious dissipation at the interface. As illustrated in Figure 2, an explicit time integrator with a fine time step Δt_1 is adopted for the subdomain Ω_1 and an implicit time integrator with a large time step Δt_2 is used for subdomain Ω_2, with $\Delta t_2 = m\Delta t_1$, m being the time step ratio between two subdomains. In this way, hybrid (different schemes associated) asynchronous (different time steps depending on subdomains) ALID can be obtained, called HA-ALID. The equilibrium of subdomain 1 is prescribed at time t_m at the end of the large time Δt_2, while the equilibrium of subdomain 2 is prescribed at every time $t_j = j\Delta t_1$ ($j = 1, 2 \ldots m$) at the fine time scale. The gluing of the velocity at the interface is written at the fine time scale.

Using the GC method, the wave propagation can be simulated using a fine time step, without being affected by the specific formulation adopted for the absorbing region at the boundary of the truncated mesh. Moreover, the multi-time step capabilities enable us to use a large time step in subdomain Ω_2. Finally, the weak form given in Equation (15) with the velocity continuity equation in Equation (16), can be expressed in the following discrete form in space and time:

$$M_1\ddot{U}_1^j + K_1U_1^j = F_1^{\text{ext},j} - L_1^T\lambda^j \text{ at time } t = t_j \tag{19}$$

$$M_1\ddot{U}_1^j + (\alpha_M M_2 + \alpha_K K_2)\dot{U}_2^m + K_2U_2^m = F_2^{\text{ext},m} - L_2^T\lambda^m \text{ at time } t = t_m \tag{20}$$

$$L_1\dot{U}_1^j + L_2\dot{U}_2^j = 0 \text{ at time } t = t_j \tag{21}$$

where M_i and K_i are the mass and the stiffness matrices of subdomains Ω_1 and Ω_2 ($i = 1, 2$). The first equation is the discrete equation of motion of subdomains Ω_1 written at time t_j (fine time scale), whereas the second equation is the discrete equations of motion of subdomains Ω_2 written at time t_m (large time scale). On right hand side of the above equations, the interface forces enable the subdomains to be glued at their interface Γ_1. The last equation is the velocity continuity.

It is important to note that the expression of the classical viscous Rayleigh damping matrix, denoted by $C_2 = \alpha_M M_2 + \alpha_K K_2$, is retrieved in the discrete equation of motion of subdomain Ω_2.

As a result, the α_M and α_K parameters introduced in the strong form of the wave equation given in Equations (1) and (2) represent the classical constant parameters of the viscous Rayleigh damping matrix. In structural dynamics, this matrix is classically introduced in the discrete equation of motion, with parameters chosen so as to match two damping ratio values at two different frequencies.

Newmark time integration schemes (Newmark, 1959) can be adopted for the time discretization, for example, characterized by the parameters $\gamma_2 = 0.5$ and $\beta_2 = 0.25$ for the implicit time integration (Constant Average Acceleration scheme) and the parameters $\gamma_1 = 0.5$ and $\beta_1 = 0$ for the explicit time integration scheme (Central Difference). By introducing the approximate Newmark formulae, it leads to the equations of motion written as:

$$\widetilde{M}_1 \ddot{U}_1^j = F_1^{\text{ext},j} - K_1 U_1^{j-1,p} - L_1^T \lambda^j \tag{22}$$

$$\widetilde{M}_2 \ddot{U}_2^m = F_2^{\text{ext},m} - C_2 \dot{U}_2^{0,p} - K_2 U_2^{0,p} - L_2^T \lambda^m \tag{23}$$

where $U_1^{j-1,p}$ and $\dot{U}_2^{0,p}$ denote the predictor values in terms of displacement and velocity, classically introduced through the approximate Newmark formulae; they correspond to quantities known at the beginning of the fine step and of the large time step, respectively.The effective stiffness matrices $\widetilde{M}_1$ and $\widetilde{M}_2$ related to the two subdomains are defined by:

$$\widetilde{M}_1 = M_1 + \beta_1 \Delta t_1^2 K_1 \tag{24}$$

$$\widetilde{M}_2 = M_2 + \beta_2 \Delta t_2^2 K_2 + \gamma_2 \Delta t_2 C_2 \tag{25}$$

The kinematic quantities are divided into two parts: the free and the linked quantities in the coupling GC method. The free quantities are calculated by taking into account the internal and external forces, without considering the interface forces, whereas the linked quantities are obtained from the interface loads given by the Lagrange multiplier vector λ.

It was demonstrated that the kinematic continuity condition can be expressed as a reduced-size interface problem as follows:

$$H\lambda^j = b_j \tag{26}$$

with the interface operator and the right-hand side member vector defined by:

$$\begin{cases} H = \gamma_1 \Delta t L_1 \widetilde{M}_1^{-1} L_1^T + \gamma_2 \Delta t L_1 \widetilde{M}_1^{-1} L_1^T \\ b_j = L_1 \dot{U}_1^{\text{free},j} + L_2 \dot{U}_2^{\text{free},j} \end{cases} \tag{27}$$

The interface operator H is called the Steklov–Poincaré operator which can be viewed as the condensed mass matrix on the degrees of freedom belonging to the interface between the two subdomains. The right hand-side vector b_j only depends on the free velocities computed in both subdomains without considering the interface forces; it can be seen as a predictor value projected to the degrees of freedom belonging to the interface.

Finally, once derived the Lagrange multiplier vector, the quantities related to the interface forces can be computed and the time step is completed by summing these linked quantities to the free quantities previously obtained.

Effectiveness of HA-ALID

In order to evaluate the effectiveness of HA-ALID, 2D Lamb's test has been simulated using Abaqus Explicit/Implicit co-simulation. In Lamb's test, the concentrated load applied to the surface of an infinite half space medium generates three types of waves propagating through the soil, involving P, S waves and Rayleigh waves (Lamb, 1903). So, 2D Lamb's test can be considered as a good test for assessing the performance of the HA-ALID using Abaqus co-simulation. Non-harmonic waves are investigated by considering a Ricker incident waves

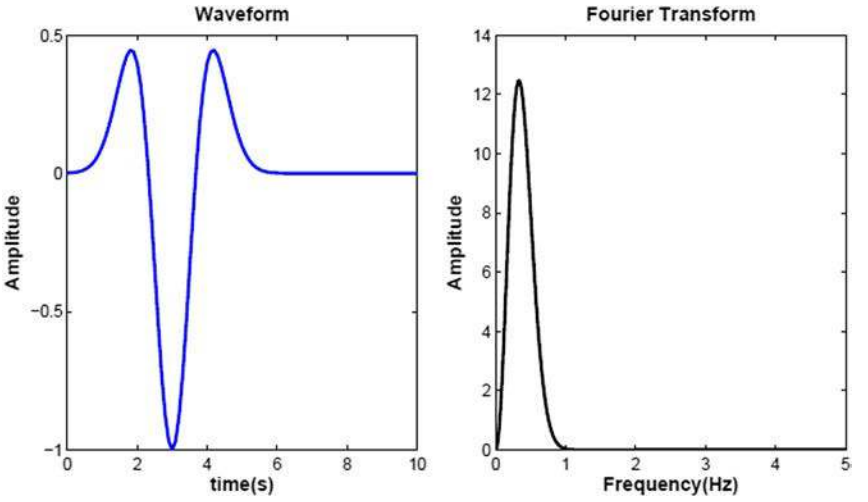

Figure 3. Waveform and Fourier transform of the Ricker wavelet.

defined by:

$$Ric(t, t_p, t_s) = A \quad 2\pi^2 \frac{(t - t_s)^2}{t_p^2} - 1 \Bigg) \exp \quad -\pi^2 \frac{(t - t_s)^2}{t_p^2} \Bigg) \tag{28}$$

The Ricker wave, plotted in time domain and in frequency domain in Figure 3, has three parameters: the fundamental period t_p, the time shift t_s and the amplitude A. The chosen values are: $t_p = 3$s, $t_s = 3$s and $A = 1$ MN. In this section, the first example of 2D Lamb's test is simulated with a single Rayleigh absorbing layer by using a homogeneous time step in both subdomains. Second, HA-ALID are tested so as to significantly reduce the scale of the absorbing medium at the boundary of the truncated mesh in comparison to the single-layer case. The effect of nonlinear increase of damping ratio and heterogeneous time steps on the accuracy will be investigated. Finally, a comparison will be carried out between results obtained by HA-ALID using Abaqus Explicit/Implicit co-simulation, infinite element using Abaqus Explicit and reference results provided by an extended mesh using Abaqus Explicit without non-reflective conditions.

Single absorbing layer

Lamb's test is set up considering a single absorbing layer as illustrated in Figure 4, composed of a bounded soil (subdomain 1) with a size of λ (wavelength of P-waves) and a single absorbing layer (subdomain 2) with the thickness of 3.6 λ, designed to achieve a target logarithmic decrement $\delta = \ln(10)$.

The soil is assumed to be linear elastic with the following material characteristics: $\rho_1 = 1700\,\text{kg/m}^3$, $E_1 = 10$ MPa and $\nu_1 = 0.24$ for the density, Young's modulus and Poisson's ratio, respectively. The material characteristics of the Rayleigh absorbing layer are computed from the optimal conditions given in Equations (6), by adopting a damping ratio $\xi = 0.1$ and taking into account a dominant angular frequency corresponding to the fundamental period t_p of the Ricker wave. It gives: $\rho_2 = 1700\,\text{kg/m}^3$, $E_2 = 9.9$ MPa, $\nu_2 = 0.24$ for the density, Young's modulus and Poisson's ratio, respectively. A homogeneous time step satisfying the CFL condition is taken in both subdomains. The subdomain soil is integrated in time with an explicit scheme, whereas the Rayleigh absorbing layer is integrated with an implicit scheme. An observation point is located at a distance d equal to 20 m from the load point. The model is spatially discretized using 4-node bilinear plane strain quadrilateral elements with the size of $\lambda/50$ for both subdomains,

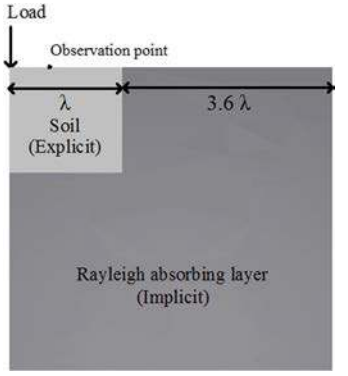

Figure 4. Lamb's test with a single absorbing layer: the soil is integrated in time with an explicit scheme and the absorbing layer with an implicit scheme.

guaranteeing a good quality of the numerical prediction for the wave propagation problem. The P-wave, S-wave and Rayleigh wave velocities are: V_P =83.27 m/s, $V_S = 48.7$ m/s, $V_R = 44.73$ m/s.

Figures 5 and 6 show the horizontal and vertical displacements in Lamb's test with a single absorbing layer in comparison to the reference results obtained from an extended mesh, free of spurious reflected waves in the observation period. The horizontal and vertical displacements of the spurious wave reflected at the interface are less than 1.5% with respect to the horizontal and vertical amplitudes of the incident wave. By comparing these results to our target equal to 1% for the reflection coefficient *R*, small discrepancies are observed, due to the non-normal incidence of waves, non-harmonic nature of the Ricker wavelet and the space-time discretization of the problem. Results obtained by Abaqus Explicit/Implicit co-simulation with a single layer and an homogeneous time step in two subdomains are in good agreement with the reference results, highlighting the excellent behaviour of the Rayleigh absorbing layer. Next, a multi-layer strategy (HA-ALID) will be used to reduce the scale of the absorbing region.

HA-ALID in Lamb's test

The HA-ALID for the Lamb's test is depicted in Figure 7. The size and material parameters of the soil domain are the same as in the previous example. We consider 10 sublayers in the absorbing region and a size of $\lambda/10$ for each sublayer; ξ_0 in Equation (9) is chosen equal to 1. Thanks to the multi-layer strategy, the thickness *e* of the absorbing region can be reduced from 3.6λ for the previous one layer case to λ. The damping ratio of each layer depends on the selected profile of the damping ratio evolution in the thickness of the HA-ALID and three types of profile are investigated: linear, quadratic and square root. The other material parameters of layers can be calculated on the basis of the optimal conditions at the interface given in Equation (9).

Influence of the evolution of the damping ratio in the HA-ALID

Due to the difference of damping ratio, spurious waves are produced at the interface between subdomain Ω_1 and Ω_2, corresponding to the HA-ALID. In the same way, spurious waves are produced between different layers of the HA-ALID. Therefore, it is crucial to control the evolution of damping ratio in layers. Three kinds of evolution functions are tested to find out which kind has the best performance: $\xi_i = \xi_0 \frac{i}{N_e}$, $\xi_i = \xi_0 (\frac{i}{N_e})^2$, $\xi_i = \xi_0 \sqrt{\frac{i}{N_e}}$. The values of damping ratio and the derived reflection coefficient corresponding to the ALID are given in Table 1. It can be noted that reflection coefficients are less than 1% for the three damping ratio profiles.

Figures 8 and 9 compare the results obtained at the observation point using different damping profiles and a homogeneous time step in comparison to the reference results obtained from

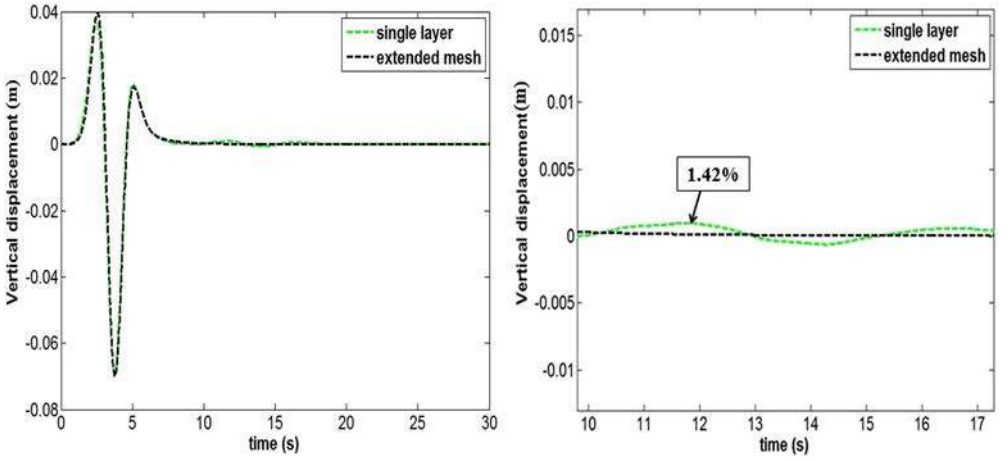

Figure 5. Vertical displacements at observation point using a single layer compared to the reference results.

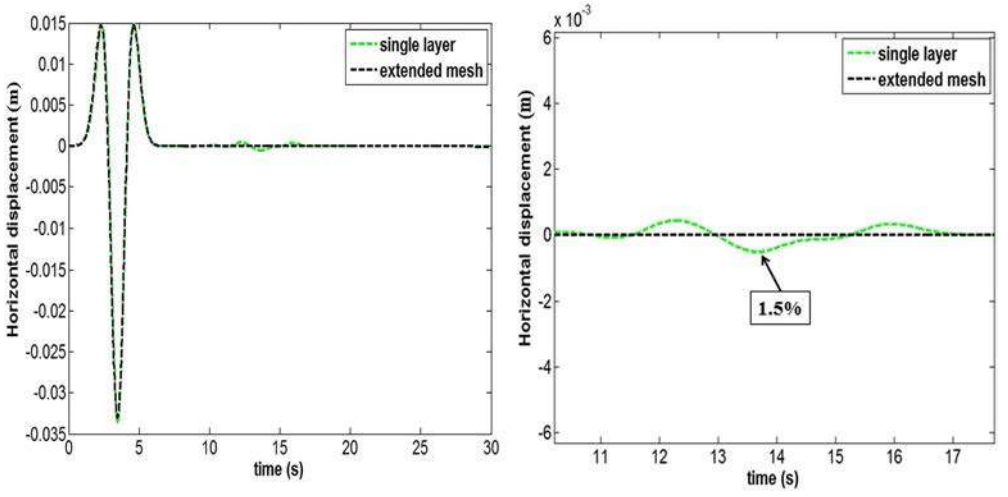

Figure 6. Horizontal displacements at the observation point using a single layer compared to the reference results.

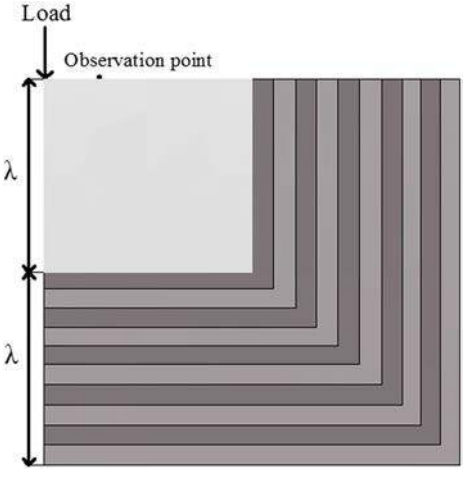

Figure 7. Lamb's test with HA-ALID: the soil is integrated in time with explicit scheme and HA-ALID with implicit scheme.

Table 1. Evolution of the damping ratio for different profiles (linear, quadratic, square-root).

	Functions		
i	$\xi_0 \frac{ie_l}{e}$	$\xi_0 (\frac{ie_l}{e})^2$	$\xi_0 \sqrt{\frac{ie_l}{e}}$
1	0.1	0.01	0.316
2	0.2	0.04	0.447
3	0.3	0.09	0.548
4	0.4	0.16	0.632
5	0.5	0.25	0.707
6	0.6	0.36	0.775
7	0.7	0.49	0.837
8	0.8	0.64	0.894
9	0.9	0.81	0.949
10	1.0	1.0	1.0
Reflection coefficient	0. 1%	0.8%	0.01%

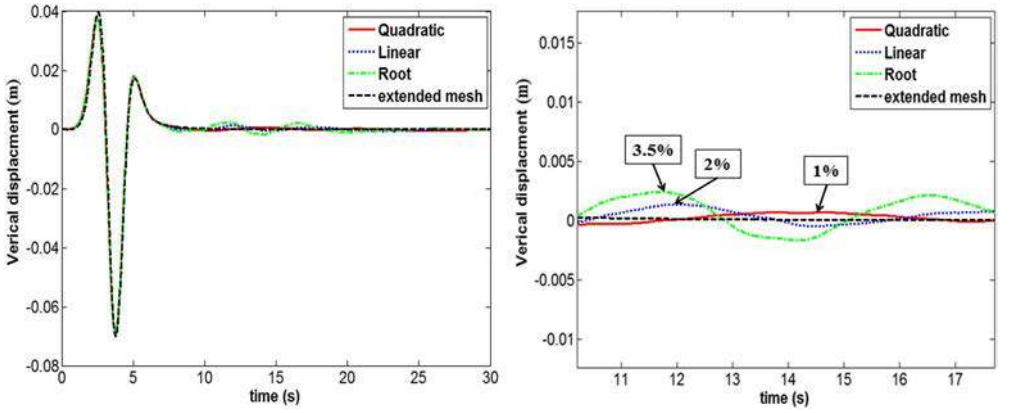

Figure 8. Vertical displacements at observation point using different damping ratio profiles.

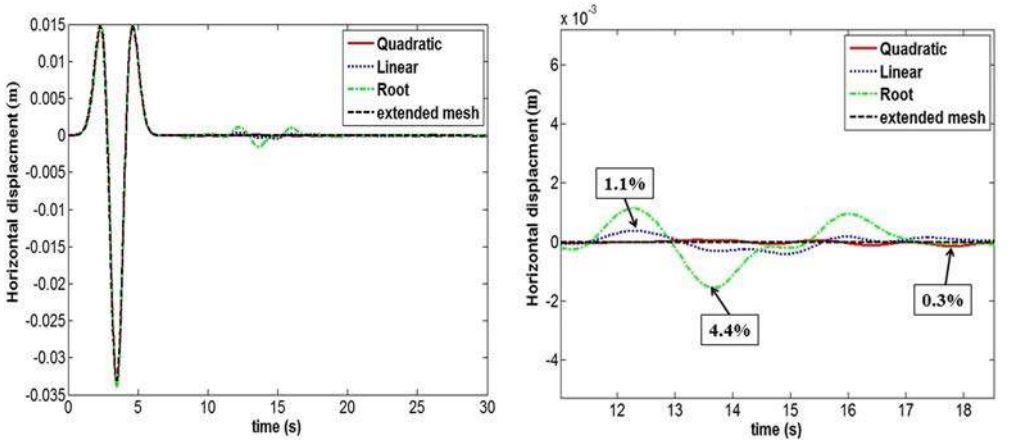

Figure 9. Horizontal displacements at the observation point using different damping ratio profiles.

the extended mesh. The horizontal and vertical displacements of the spurious waves reflected at the interface by using the quadratic function performs best: 0.3% with respect to the horizontal amplitude of the incident wave and 1% with respect to the vertical amplitude of the incident wave, even though its reflection coefficient based on Equation (11) is the biggest as seen in Table 1 (0.8% in comparison to 0.1% and 0.01% for the two others).

The results obtained with the linear function are better than that of the square root function. It highlights that the evolution of damping ratio in layers has an important influence on the

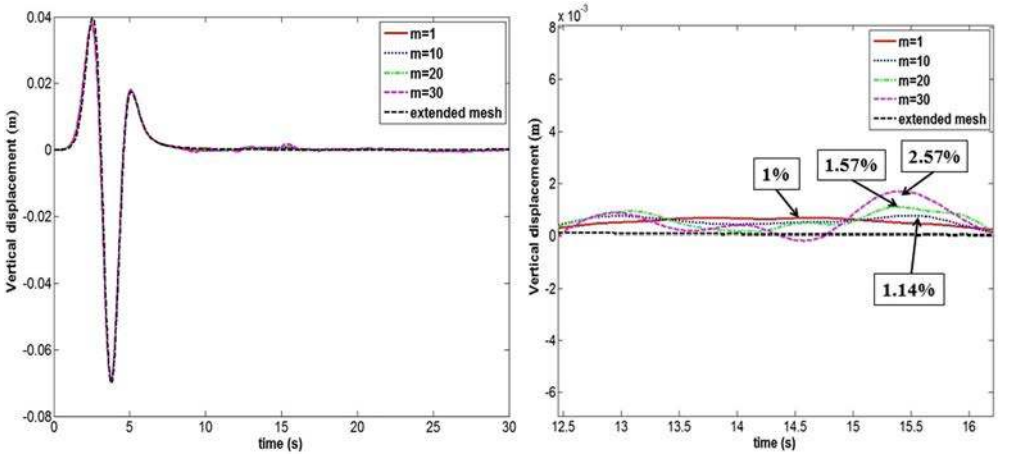

Figure 10. Vertical displacements at the observation point using different time step ratios *m*.

performance of HA-ALID. The difference of damping ratios between subdomain Ω_1 and the first layers of the HA-ALID Ω_2 is the smallest by using the quadratic function: this is certainly why the best results are obtained by the quadratic function. The bigger the difference of damping ratios between subdomain Ω_1 and Ω_2 is, the bigger spurious waves are produced, even though Young's modulus is modified so as to satisfy the optimal non-reflective conditions in Equation (9) for harmonic waves with normal incidence. It can also be remarked that the difference of damping ratio for the last sublayers provided by the quadratic function grows bigger than that of linear function or square root function. However, the generated spurious waves from the last layers have little impact on the global results, because the spurious waves caused by these last layers are strongly attenuated by the others layers before coming back into the domain of interest.

Effect of the time ratio on the accuracy of the HA-ALID

The subdomain soil and HA-ALID are integrated with an explicit scheme and an implicit scheme, respectively. A homogeneous time step can be adopted, which satisfies the CFL condition without damping. Indeed, using the implicit time integration for the HA-ALID, we avoid the decrease of the critical time step in the explicit framework due to the introduction of the Rayleigh damping into the discrete equation of motion, as it is noted in Abaqus/Explicit documentation (ABAQUS, 2013). Moreover, as explained in section 'Hybrid asynchronous Rayleigh absorbing layer', it is possible to use a larger time step in HA-ALID, because we use an unconditionally stable implicit scheme.

In this part, the subdomain soil is integrated with Abaqus/Explicit with a fine time step, whereas the HA-ALID are dealt with Abaqus/Implicit associated with a large time step in order to reduce the computation time.

The horizontal and vertical displacements of the observation point with different time step ratios m ($\Delta t_2 = m\Delta t$) equal to 10, 20 and 30, are shown in Figures 10 and 11. The kinetic and internal energies are computed for different time step ratios as shown in Figure 12. In order to distinguish the difference between them, the L^2 norm error in time is computed between energies of HA-ALID and those of extended mesh (reference results). Considering a quantity E over the time interval [0, T], the L^2 norm is defined by:

$$\text{err} = \frac{\|E^{(m)} - E_{\text{ref}}\|_{L^2([0,T])}}{\|E_{\text{ref}}\|_{L^2([0,T])}} \tag{29}$$

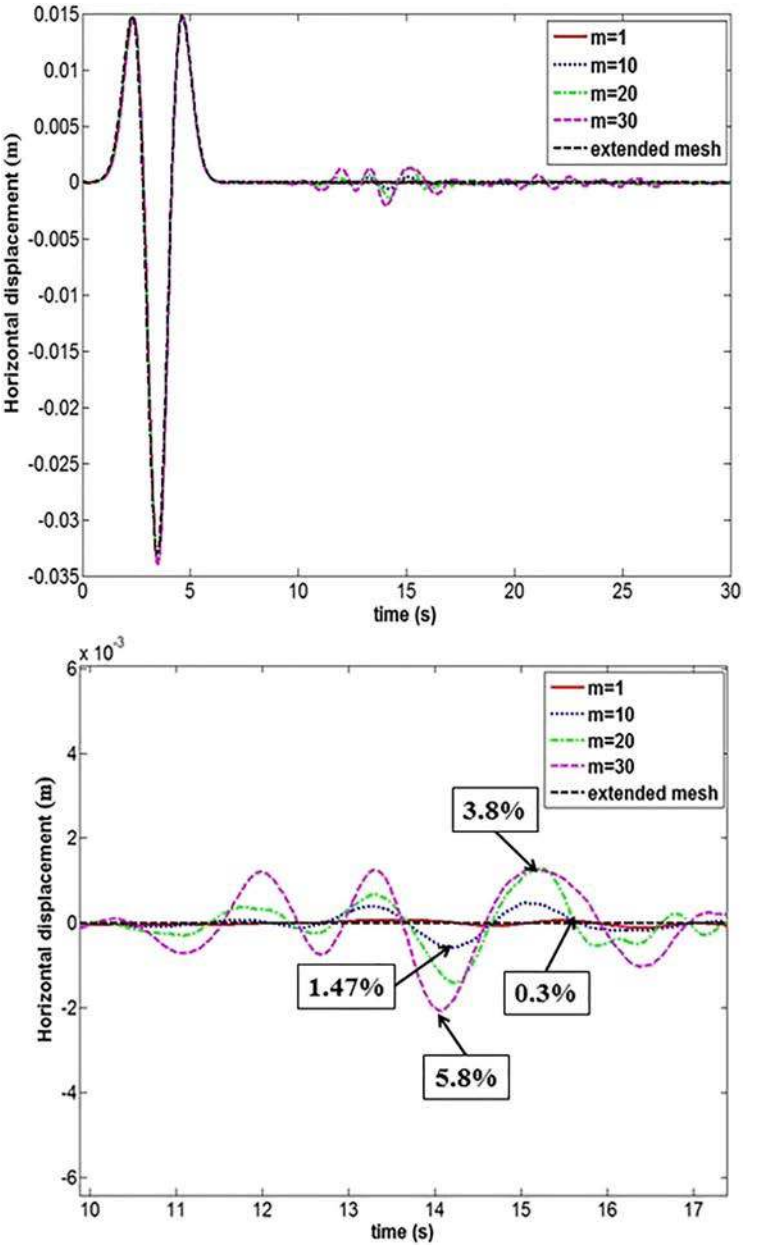

Figure 11. Horizontal displacements at the observation point using different time step ratios *m*.

$E^{(m)}$ is the kinetic or internal energy obtained by Abaqus Explicit/Implicit co-simulation with the time step ratio m and E_{ref} is the reference energy obtained from the extended mesh.

The reflected spurious waves recorded at the observation point grow bigger with the increase of the time step ratio m. It can be observed that in comparison to the displacements given by reference results, the vertical amplitude of the spurious wave varies from 1% to 2.57% with respect to the vertical amplitude of the incident wave, while the horizontal amplitude of the spurious wave varies from 0.3% to 5.8% with respect to that of the incident wave. From Table 2, it can be noted that the error in kinetic energy increases from 0.48% to 1.12% when the time step ratio increases from 1 to 30, whereas the error in internal energy increases from 0.43% to 0.95%. It can be observed that the errors remain small and stable in terms of energy.

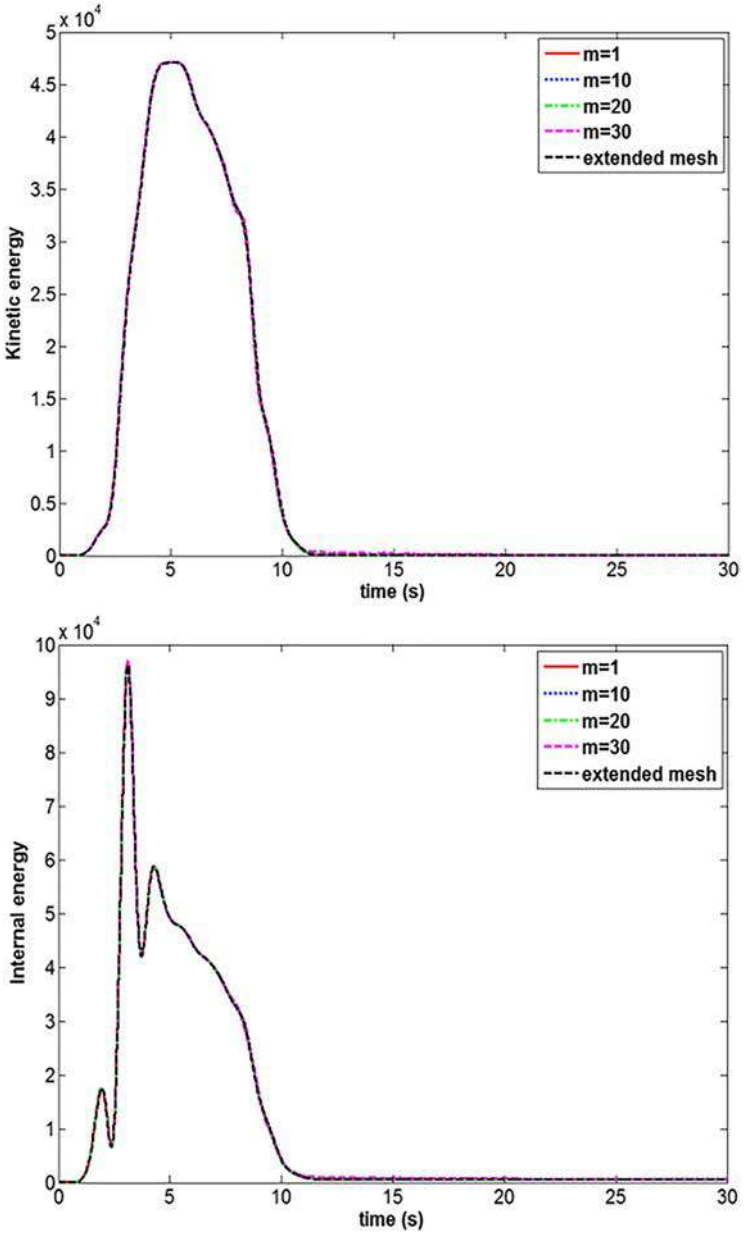

Figure 12. Kinetic and internal energies computed using different time step ratios compared to the reference results using an extended mesh.

Table 2. Relative errors of different time step ratio.

	Kinetic energy (%)	Internal energy (%)
$m = 1$	0. 48	0.43
$m = 10$	0.67	0.45
$m = 20$	0.77	0.63
$m = 30$	1.12	0.95

Table 3. Material properties of soil and barrier.

Material	Density ρ (kg/m^3)	Poisson's ratio ν	Young's modulus E (GPa)	Damping ratio B
Soil	1750	0.25	0.33	0
Barrier	2397.5	0.25	11.30	0

Based on these results, the time step ratio m has to be chosen under 10 without significant influence on the accuracy of HA-ALID. The observed decrease of accuracy as the time step ratio increases can be explained by the following points. First, due to the increase of the time step in the implicit scheme, the numerical errors grow. Second, the GC coupling algorithm is known to be dissipative as soon as heterogeneous time steps are used between the subdomains, generating spurious waves at the interface.

Comparison between infinite elements and Rayleigh absorbing layers in Abaqus

Infinite elements available in Abaqus/Explicit allow to deal with unbounded media. To further validate the accuracy of the HA-ALID using Abaqus Explicit/Implicit multi time step co-simulation, we compare their performance with infinite elements available in Abaqus/Explicit. Thus, a numerical model is established using Abaqus/Explicit with the same mesh and materials than our previous explicit/implicit simulations: HA-ALID are just replaced with Abaqus infinite elements.

The horizontal and vertical displacements of three numerical models at the observation point are shown in Figures 13 and 14. We can observe that the results obtained by Abaqus Explicit/Implicit co-simulation and reference results are in a good agreement: the reflected spurious wave is 1.47% in terms of the horizontal displacement, 1.14% in terms of the vertical displacement when the time step ratio m is equal to 10. In comparison, the reflected spurious wave produced by infinite element is equal to 10.4% with respect of the vertical amplitude of the incident wave and 17.6% with respect of the horizontal amplitude of the incident wave. In conclusion, HA-ALID has a much better accuracy than Abaqus infinite elements. In the following section, the relevance of the proposed HA-ALID will be assessed in the case of a wave barrier problem.

An application in wave barrier numerical simulation

Due to the increasing vibrations caused by human activities, the performance of wave barriers for reducing the distress to adjacent structures and annoyance to people, have been studied for more than 30 years. As illustrated in Figure 15, the wave barrier configuration studied by Beskos, Dasgupta, and Vardoulakis (1986) and Al-Hussaini and Ahmad (1991) is investigated. In this case, it was shown that the major part of the vibration energy is transferred by Rayleigh waves which may cause strong ground motions on nearby structures. An application of HA-ALID is carried out for this case of wave barrier.

In this soil–barrier configuration, D is the depth of the barrier, equal to 5 m, W is the width of the barrier, equal to 0.5 m, L_1 is the distance from the dynamic load to the barrier equal to 25 m and L_2 is the distance from the barrier to the point of interest equal to 25 m. The total length of the model is 120 m and the depth is 25 m. The inclination angle U of the barrier is given as 90°. A dynamic load P with a width of r equal to 1.25 m is applied to the left top surface of the soil, producing a Rayleigh wave to simulate dynamic events such as the compaction, blasting and seismic waves. The dynamic periodic load in the numerical model is $P = P_0 \cos(\omega_0 t), \omega_0 = 100\pi$, $P = 1000$ N, the material properties of soil and barrier are shown in Table 3. In the soil, the P-wave, S-wave and Rayleigh-wave velocities are: $V_P = 475.7$ m/s, $V_S = 274.64$ m/s, $V_R = 252.62$m/s. In order to achieve a good accuracy in predicting the propagating waves into the soil, the finite element size is kept as $\lambda_P/50$ for both subdomains.

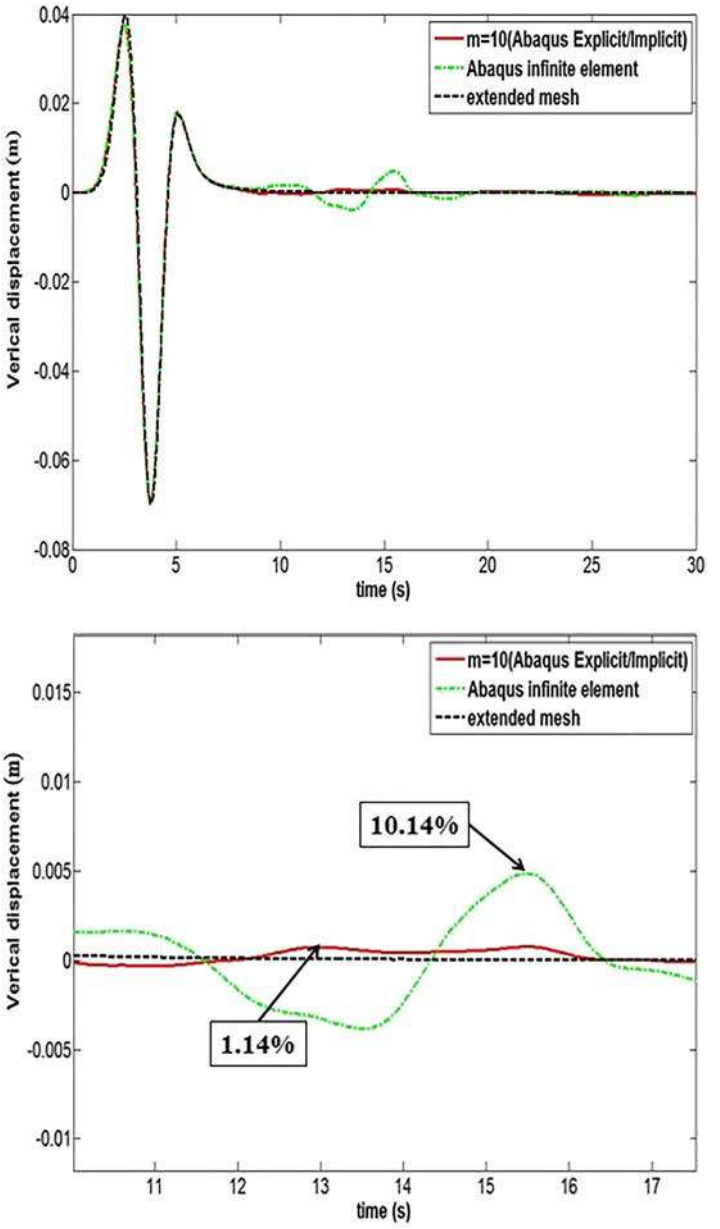

Figure 13. Vertical displacements at the observation point using different methods.

HA-ALID adopts a quadratic evolution of damping ratio. Taking advantage of the partition strategy through Abaqus Explicit/Implicit co-simulation, the 2D soil–barrier system is divided into three partitions integrated in time with their own time integrator and time step: soil subdomain (explicit scheme), barrier subdomain (implicit scheme, with a large time step ratio *m* equal to 10), Rayleigh absorbing layers subdomain (implicit scheme, with a large time step ratio m equal to 10), as shown in Figure 16.

In the solid barrier, the P-wave velocity is equal to 2378.21 m/s. In a full explicit computation using Abaqus/Explicit, the time step must satisfy the smallest time step depending on finite element sizes and material characteristics. HA-ALID involve large values of damping ratios for absorbing the incident waves. In Abaqus/Explicit documentation, recommended values are

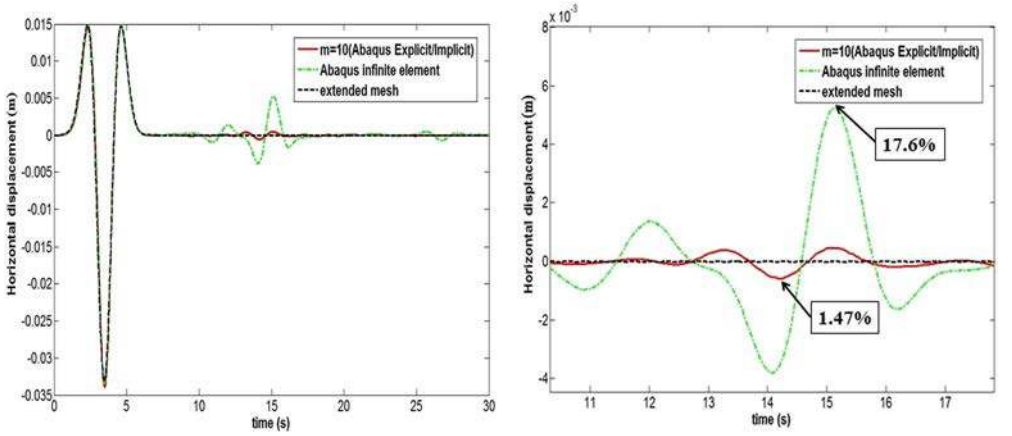

Figure 14. Horizontal displacements at the observation point using different methods.

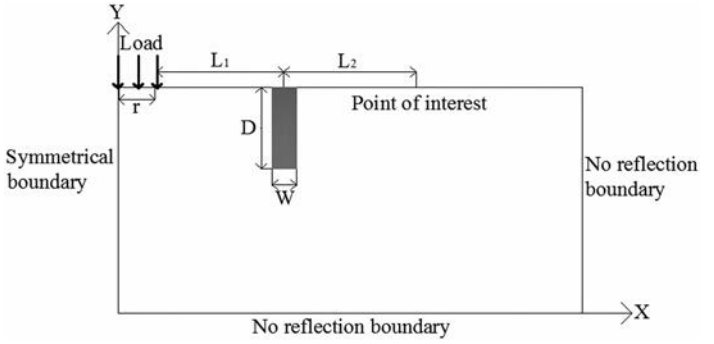

Figure 15. Investigated configuration of a 2D soil–barrier system.

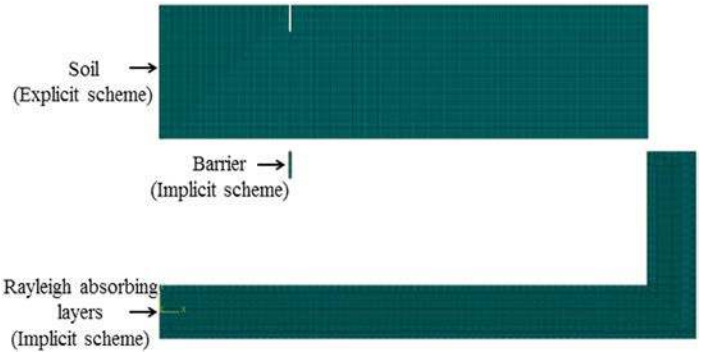

Figure 16. Wave-barrier model split in three partitions: soil, solid barrier, ALID.

provided so as to guarantee the stability of the explicit time integration scheme:

$$\Delta t \leq \frac{2}{w_{\max}}\left(\sqrt{1+\xi_{\max}^2}-\xi_{\max}\right) \tag{30}$$

$$\xi_{\max} = \frac{\alpha_M}{2w_{\max}} + \frac{\alpha_K w_{\max}}{2} \tag{31}$$

Applying the above formulae to the layers composing the ALID leads to a strong decrease of the critical time step in a full explicit computation. Table 4 resumes the critical time steps depending

Table 4. Critical time steps for each partition in full explicit computations.

Soil	Barrier	Rayleigh layers	Time step adopted
269×10^{-6}	53.8×10^{-6}	27.5×10^{-6}	27.5×10^{-6}

Table 5. Critical time steps for each partition in explicit/implicit multi time step co-simulations.

Soil	Barrier	Rayleigh layers
250×10^{-6}	2500×10^{-6}	2500×10^{-6}

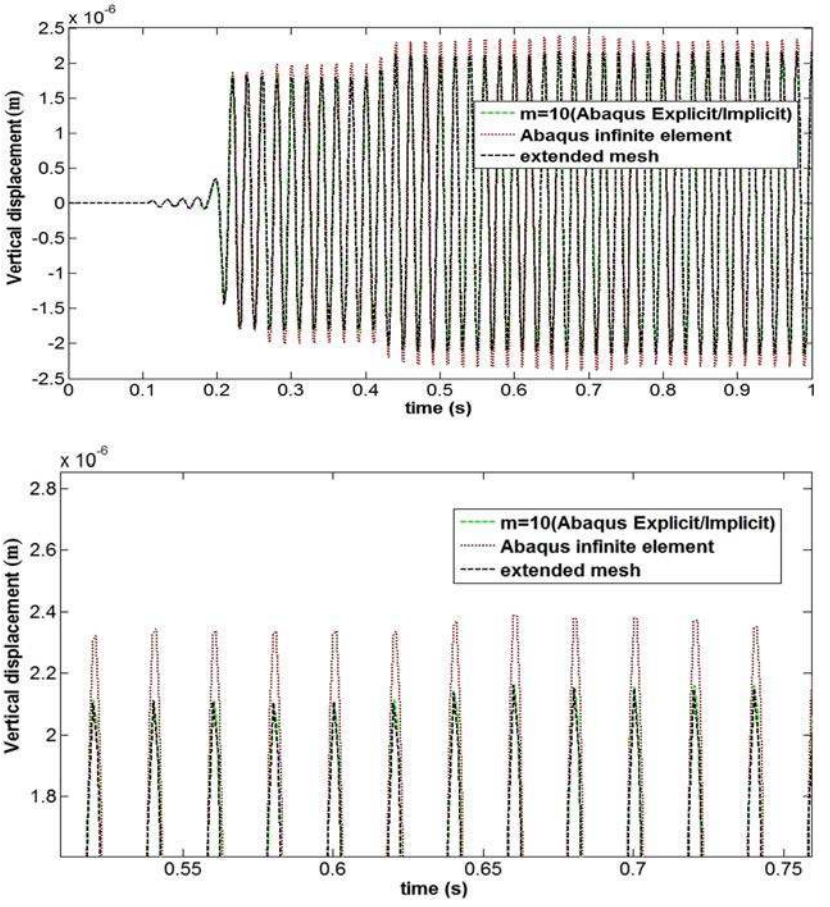

Figure 17. Vertical displacements and local zoom at the observation point using HA-ALID with $m = 10$ and infinite elements in a full explicit computation, compared to the reference results (extended mesh).

on the partition under consideration (soil, barrier, ALID). It can be noted that ALID have a large impact on the time step size.

When adopting HA-ALID using Abaqus Explicit/Implicit multi-time step co-simulation, the critical time step in the soil is unaffected by the models of the solid barrier and the HA-ALID. Time step sizes for the different partitions are given in Table 5, highlighting the interest of the co-simulation. Using HA-ALID, a time step equal to 250×10^{-6} s can be used in the soil, whereas a full explicit computation requires a value of 27.5×10^{-6} s related to the absorbing layers.

Figure 17 shows the vertical displacements of the observation point with HA-ALID, compared to the results obtained using infinite elements with the same configuration and the reference results obtained from an extended mesh free of spurious reflected waves from the boundary during the observation period. It turns out that the results of HA-ALID agree well with the

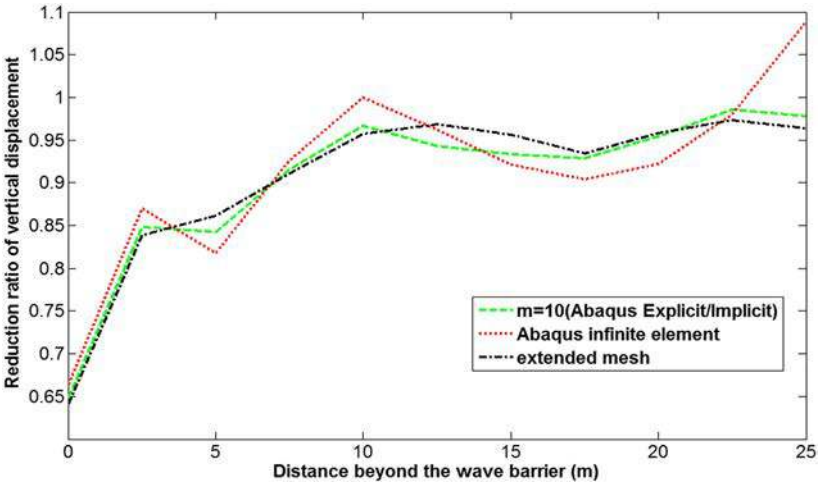

Figure 18. Reduction ratio of vertical displacements using HA-ALID with $m = 10$ and infinite elements in a full explicit computation, compared to the reference results (extended mesh).

reference results, contrary to the full explicit computation with infinite elements: the errors in terms of vertical displacements obtained using infinite elements can be greater than 10%, whereas the biggest error with HA-ALID is equal to 2.7% with respect to the amplitude of reference results.

The isolation effect of the installation of the barrier can be assessed by the parameter A_r (amplitude reduction ratio), which provides a quantitative evaluation of the screening effect of the barrier. Its expression is given by: $A_r = A_b/A_s$, where A_b is the displacement amplitude with the barrier and A_s the displacement amplitude without the barrier. For example, $A_r = 0.8$ means that 20% reduction of the vibration has been reached due to the installation of the barrier. The reduction ratio of vertical displacement on the surface beyond the barrier can be plotted in Figure 18, for the three computations. From this figure, it can be concluded that the reduction ratios obtained by HA-ALID have a better agreement with the reference results than those obtained by infinite elements.

Conclusion

In the context of wave simulation in the soil, ALID can be easily set up for damping out the incident waves at the boundary of a finite element mesh thanks to the availability of the viscous Rayleigh damping matrix in commercial FE codes. In this article, a simple and accurate method for modelling unbounded domains is proposed using explicit/implicit co-simulation. Subdomain decomposition strategy is applied for problems coupling physical medium with Rayleigh absorbing layers, based on the GC method. The co-simulation strategy involving different FE codes with their own time integrator and time step has been employed for the simulation of wave barrier problem using the Abaqus package: the soil partition in which we desire an accurate prediction of the wave propagation has been handled by Abaqus/Explicit with a fine time step, whereas the other partitions, the solid barrier and the HA-ALID (Hybrid Asynchronous ALID), employed for modelling the semi-infinite soil medium, have been dealt with Abaqus/Implicit with a large time step.

In order to highlight the accuracy of the method, 2D Lamb's test and a wave barrier problem have been studied using HA-ALID with a quadratic profile of damping ratio in the thickness direction of the HA-ALID. Very satisfactory results have been achieved in terms of kinematic quantities and energies. The obtained results showed that spurious waves reflected at the boundary of

the truncated mesh are much lower than the ones generated by non-reflective conditions available in Abaqus/Explicit for modelling infinite medium (infinite elements). On the other hand, some interesting benefits of the HA-ALID can be underlined in comparison to the classical ALID. First, large time steps can be adopted in the solid barrier and in the HA-ALID in comparison to the fine time step in the soil medium corresponding to the CFL condition. Second, the critical time step in the soil partition is unaffected by the choice of damping matrix in the layers of the HA-ALID, related to the stiffness or mass matrices, contrary to the case of a full explicit computation for which the critical time step can be significantly reduced.

As a conclusion, because of its good accuracy and ability to be realized in Abaqus package without a third-party software, the proposed HA-ALID has a wide range of applications for modelling wave propagation problem involving unbounded domains. The 2D wave barrier problem studied in this paper is a first example. Future work will consider wave propagation in 3D media for soil–structure interaction problems, by comparing the advantages of HA-ALID and HA-PML (Hybrid Asynchronous Perfect Matched Layers) recently proposed by Brun, Zafati, Djeran-Maigre, and Prunier (2016).

References

ABAQUS. (2013). *Abaqus analysis user's guide*. USA: Dassault Systèmes.

Al-Hussaini, T. M., & Ahmad, S. (1991). Simplified design for vibration screening by open and in-filled trenches. *Journal of Geotechnical and Geoenvironmental Engineering, ASCE*, *117*(1), 67–88.

Basu, U., & Chopra, A. (2010). Perfectly matched layers for transient elastodynamics of unbounded domains. *International Journal for Numerical Methods in Engineering*, *59*, 1039–1074.

Bérenger, J. P. (1994). A perfectly matched layer for the absorption of electromagnetic waves. *Journal of Computational Physics*, *114*, 185–200.

Beskos, D. E., Dasgupta, B., & Vardoulakis, I. G. (1986). Vibration isolation using open or filled trenches. *Computational Mechanics*, *1*, 43–63.

Bettess, P. (1977). Infinite elements. *International Journal for Numerical Methods in Engineering*, *11*, 53–64.

Brun, M., Batti, A., Combescure, A., & Gravouil, A. (2014). External coupling software based on macro-and micro-time scales for explicit/implicit multi-time-step co-computations in structural dynamics. *Finite Elements in Analysis and Design*, *86*, 101–119.

Brun, M., Batti, A., Limam, A., & Combescure, A. (2012). Implicit/explicit multi-time step co-computations for predicting reinforced concrete structure response under earthquake loading. *Soil Dynamics and Earthquake Engineering*, *33*, 19–37.

Brun, M., Batti, A., Limam, A., & Gravouil, A. (2012). Explicit/implicit multi-time step co-computations for blast analyses on a reinforced concrete frame structure. *Finite Elements in Analysis and Design*, *52*, 41–59.

Brun, M., Gravouil, A., Combescure, A. & Limam, A. (2015). Two FETI-based heterogeneous time step coupling methods for Newmark and α-schemes derived from the energy method. *Computer Methods in Applied Mechanics and Engineering*, *283*, 130–176.

Brun, M., Zafati, E., Djeran-Maigre, I., & Prunier, F. (2016). Hybrid asynchronous perfectly matched layer for seismic wave propagation in unbounded domains. *Finite Elements in Analysis and Design*, *122*, 1–15.

Çelebi, E., Fırat, S., Beyhan, G., Çankaya, İ., Vural, İ., & Kırtel, O. (2009). Field experiments on wave propagation and vibration isolation by using wave barriers. *Soil Dynamics and Earthquake Engineering*, *29*, 824–833.

Combescure, A., & Gravouil, A. (2002). A numerical scheme to couple subdomains with different time-steps for predominantly linear transient analysis. *Computer Methods in Applied Mechanics and Engineering*, *191*, 1129–1157.

Enquist, B., & Majda, A. (1977). Absorbing boundary conditions for the numerical simulation of waves. *Mathematics of Computation*, *31*, 629–651.

Gravouil, A., & Combescure, A. (2001). A multi-time-step explicit–implicit method for non-linear structural dynamics. *International Journal for Numerical Methods in Engineering*, *50*, 199–225.

Hughes, T. J. R. (1987). *The finite element method: Linear static and dynamic finite element analysis*. Englewood Cliffs, NJ: Prentice-Hall.

Lamb, H. (1903). On the propagation of tremors over the surface of an elastic solid. *Proceedings of the 38th Royal Society of London*, *72*, 128–130.

Nasri, V., & Magnan, J. P. (1997). Éléments infinis dans les problèmes de consolidation. *European Journal of Environmental and Civil Engineering*, *1*(4), 667–685.

Newmark, N. M. (1959). A method of computation for structural dynamics. *Journal of the Engineering Mechanics Division (ASCE)*, *85*, 67–94.

Nunez-Ramirez, J., Marongiu, J. C., & Brun, M. (2017). A partitioned approach for the coupling of SPH and FE methods for transient nonlinear FSI problems with incompatible time-steps. *International Journal for Numerical Methods in Engineering*, *109*, 1391–1417.

Rajagopal, P., Drozdz, M., Skelton, E. A., Lowe, M. J. S., & Craster, R. V. (2012). On the use of the absorbing layers to simulate the propagation of elastic waves in unbounded isotropic media using commercially available finite element packages. *NDT & E International*, *51*, 30–40.

Semblat, J. F. (1999). Validation des calculs de propagation d'ondes: Approches par éléments finis et éléments de frontière. *European Journal of Environmental and Civil Engineering*, *3*(7–8), 565–575.

Semblat, J. F., Lenti, L., & Gandomzadeh, A. (2011). A simple multi-directional absorbing layer method to simulate elastic wave propagation in unbounded domains. *International Journal for Numerical Methods in Engineering*, *85*, 1543–1563.

Su, J., & Wang, Y. (2013). Equivalent dynamic infinite element for soil-structure interaction. *Finite Elements in Analysis and Design*, *63*, 1–7.

Zafati, E., Brun, M., Djeran-Maigre, I., & Prunier, F. (2014). Multi-directional and multi-time step absorbing layer for unbounded domain. *Comptes Rendus Mécanique*, *342*, 539–557.

Zafati, E., Brun, M., Djeran-Maigre, I., & Prunier, F. (2015). Design of an efficient multi-directional explicit/implicit Rayleigh absorbing layer for seismic wave propagation in unbounded domain using a strong form formulation. *International Journal for Numerical Methods in Engineering*, *106*, 83–112.